New Journal of Physics
The open access journal for physics

The effect of van der Waal's gap expansions on the surface electronic structure of layered topological insulators

S V Eremeev[1,2], M G Vergniory[3,4,6], T V Menshchikova[2], A A Shaposhnikov[2] and E V Chulkov[3,5]

[1] Institute of Strength Physics and Materials Science, pr. Akademicheskiy 2/4, Tomsk, 634021 Russia
[2] Tomsk State University, pr. Lenina 36, Tomsk, 634021 Russia
[3] Donostia International Physics Center (DIPC), Paseo de Manuel Lardizabal, 4, 20018 San Sebastián/Donostia, Basque Country, Spain
[4] Max Planck Institute für Mikrostrukturphysik, Weinberg 2, D 06120 Halle, Germany
[5] Departamento de Física de Materiales UPV/EHU, Centro de Física de Materiales CFM-MPC and Centro Mixto CSIC-UPV/EHU, 20080 San Sebastián Donostia, Basque Country, Spain
E-mail: mgarcia@mpi-halle.de

New Journal of Physics **14** (2012) 113030 (13pp)
Received 21 June 2012
Published 22 November 2012
Online at http://www.njp.org/
doi:10.1088/1367-2630/14/11/113030

Abstract. On the basis of relativistic *ab initio* calculations, we show that an expansion of van der Waal's (vdW) spacings in layered topological insulators caused by intercalation of deposited atoms, leads to the simultaneous emergence of parabolic and M-shaped two-dimensional electron gas (2DEG) bands as well as Rashba-splitting of the former states. The expansion of vdW spacings and the emergence of the 2DEG states localized in the (sub)surface region are also accompanied by a relocation of the topological surface state to the lower quintuple layers, that can explain the absence of inter-band scattering found experimentally.

[6] Author to whom any correspondence should be addressed.

TH-2012-51

Contents

1. Introduction

Recently discovered three-dimensional topological insulators (TIs) belong to a class of insulators in which the bulk gap is inverted due to strong spin–orbit interaction [1–3]. A direct consequence of such a bulk band structure arises at the surface: the spin-polarized topologically protected massless metallic states form a Dirac cone. These surface states (SS) exhibit many interesting properties resulting from the fact that the spin of an electron is locked perpendicular to its momentum, forming an SS spin structure that protects electrons from back-scattering. This makes TIs potentially promising materials for the realization of new quantum devices.

By now several families of TIs have been discovered [4–13], of which the binary layered compounds Bi_2Te_3, Bi_2Se_3 and Sb_2Te_3 are the most studied both experimentally [10–13] and theoretically [3, 14–21]. The less studied TIs are the ternary TIs $Bi(Sb)_2Se(Te)_2Te(Se, S)$ [19, 20, 22–26, 27–29]. The latter systems, as well as the binary compounds, have a tetradymite-like layered structure with ionic-covalent bonded quintuple layer (QL) slabs, which are linked by weak van der Waal's (vdW) forces. Another family of layered TIs are the ternary systems $A^{IV}B^{VI} - mA^{V}_{2}\ B^{VI}_{3}$ ($A^{IV} = Ge, Sn, Pb$; $A^{V} = Bi, Sb$; $B^{VI} = Te, Se$). In contrast to Bi_2Se_3-type compounds, whose structure is formed by QLs, the structure of $A^{IV}\ B^{VI} - mA^{V}_{2}\ B^{VI}_{3} (m = 1)$ contains septuple layer (SL) slabs, while the $(m = 2, 3)$ compounds in this series are formed by combining QL and SL building blocks [9, 30, 31]. Such layered structures predetermine the formation of the surface by cleavage on the vdW spacing that does not result in the formation of dangling bonds, and thus only the Dirac states reside in the bulk energy gap.

However, recently in several studies it has been demonstrated, by using angle-resolved photoemission spectroscopy (ARPES), that in addition to the Dirac cone, two-dimensional electron gas (2DEG) states arise at the surface of Bi_2Se_3, Bi_2Te_3 and $Bi_2Se_{0.4}Te_{2.6}$ after a few hours of exposition in a vacuum [32], upon deposition of various magnetic [33–35] and non-magnetic atoms [34, 36, 37], and molecules as well [36, 38, 39]. In the case of Bi_2Se_3 [32–34, 36–39] these states form a parabolic band (PB) in the energy gap just below the conduction band and an M-shaped band in the local gap of the bulk-projected valence band. The former bands show an appreciable Rashba spin-splitting [33, 34, 37–40]. Moreover, for several adsorbates [34, 37, 39] at the saturation deposition time, a second and even a third pair of spin-split parabolic states emerges below the conduction band minimum. In most of these publications, the emergence of PB states was ascribed to a confinement of the conduction band states in a quantum well formed by band-bending potential produced by the adsorption of metallic atoms or residual gases, although in [38] it was pointed out that the potential gradient from band-bending cannot alone be responsible for their Rashba-splitting. Indeed, a model calculation exploiting the band-bending approach based on the coupled solution of the Poisson

and Schrödinger equations yielded the Rashba spin–orbit coupling parameter α_R considerably smaller than that extracted from the ARPES data [40]. In [40, 41] a static dielectric constant ε_0, significantly smaller than the experimentally known value [42], was used to reproduce the observed energies of the 2DEG states within the band-bending model. Furthermore, different band-bending simulations [33, 41] produce the split of the topologically protected state of the conduction band in the entire Brillouin zone that contradicts its topological nature: it should connect the bulk-valence and conduction bands. Also, the band-bending model cannot explain the most surprising experimental finding: the absence of inter-band scattering of the Dirac state electrons in the presence of the PB spin-split states after the deposition of any kind of metallic atoms [34]. A study of a naturally aged surface of Bi_2Se_3 also reveals that the scattering rate in the topologically protected state is unaffected by the potential created by adsorbed atoms or molecules [43]. In the case of Bi_2Te_3, the results are slightly different [35, 39]. Both groups have reported discrete M-shaped bands at the top of the valence band. In their discussion, Chen *et al* [39] stated the band-bending picture could not reproduce their data because the total band width of the Bi_2Te_3 valence band is larger than that of the band-bending depth and the picture proposed in [32] is not a general picture to explain the formation of the 2DEG in all the layered TIs.

It is well-known that the interlayer gaps (vdW spacings) in the layered compounds can serve as natural containers for impurities in synthesis processes and for intercalated atoms. Various atoms have been intercalated in different layered materials, inducing a giant expansion of vdW spacings [44–49]. One would expect that, due to a weak binding between QLs (SLs), even a relatively small concentration of contaminants in the vdW gap can produce its sizeable expansion. The magnitude of this expansion depends on the impurity size and on the formation of impurity atomic clusters within the vdW gap. Mechanisms of diffusion of adsorbed atoms into the vdW gap are not known in detail yet, however, at least two kinds of diffusion processes can be anticipated. First, the Fermi level of naturally grown crystals of the tetradymite-like TI is usually found to be located in the bulk conduction band due to vacancy defects [10, 13] and, thus, apparently there is a sufficiently high vacancy concentration to ensure the vacancy mediated penetration of impurities through a QL into the vdW gap. The second process can be associated with the sliding of impurity atoms into the vdW gap from the step edges. The observation of easy intercalation of the deposited atoms (Cu and Ag) onto Bi_2Se_3 [50, 51] supports the latter process. In particular, it was shown that the activation energy for the diffusion of Cu atoms in the vdW gap is almost the same as that on the flat surface and intercalation of the deposited atoms was observed.

In this work we show using *ab initio* density functional theory (DFT) calculations, that the driving mechanism of the simultaneous emergence of the parabolic and M-shaped bands in the layered TIs, Bi_2Se_3, Bi_2Te_3, Sb_2Te_3, Sb- and Bi-based ternary compounds as well as in $PbBi_2Te_4$, is an expansion of the outermost vdW spacing. The plausibility of this scenario is confirmed by the absence both of PB and M-shaped bands under the metal atom deposition on $TlBiSe_2$, which does not exhibit a layered structure [51]. This scenario also explains the Rashba-type splitting for the PB. We find that besides the emergence of PB states, which are localized in the detached QL(SL), the expansion of the vdW spacing results in a relocation of the Dirac state to the lower QL(SL) that makes the topological and PB states separated in space. This fact explains the observable absence of inter-band scattering [34, 43]. We also show that the expansion of various vdW gaps produces multiple 2DEG states in the layered TIs.

In contrast, any vdW expansion does not lead to the emergence of PB states in the energy gap of non-topological layered materials.

2. Results and discussion

We first consider the Bi_2Se_3 surface. The $A_2^{V}B_3^{VI}$ group has a rhombohedral crystal structure with five atoms in the unit cell, which can also be represented as a hexagonal structure with 15 atoms in the unit cell. Along the trigonal z-axis, atomic layers form quintuple blocks with predominantly ionic and covalent bonds inside the QLs and vdW forces between them [57].

For the electronic structure calculations, we employed the DFT with the generalized gradient approximation of [52] for the exchange-correlation potential as implemented in the Vienna ab-initio simulation package (VASP) [53, 54]. The interaction between the ion cores and the valence electrons is described by the projector augmented-wave method [55]. The Hamiltonian contains scalar relativistic corrections, and the spin–orbit coupling is taken into account by the second variation method [56]. For this system we use a slab composed of 9QL (45 atomic layers) separated by 12 Å vacuum space. For the Brillouin-zone integration we use a $11 \times 11 \times 1$ k-point grid.

To simulate the effect of both the adsorbate deposition time and the impurity atom size, we now perform calculations of the Bi_2Se_3 surface with an expansion of the outermost vdW spacing by 10–50%. Note that the large expansions can be realized in the case of the formation of atomic clusters or molecules within the vdW gap, while moderate expansions (10–20%), which are in the range of 0.24–0.48 Å, are realistic for the majority of the intercalating metal atoms.

As one can see in figure 1, the detachment of the outermost QL leads to the simultaneous emergence of both the Rashba-split band below the bottom of the bulk conduction band and the M-shaped band in the valence bulk-projected gap. The energy both of the M-shaped and parabolic spin-split bands as well as the magnitude of the Rashba splitting parameter of the PB depend strongly on the magnitude of the vdW spacing expansion. At a 10% expansion, a pair of spin-split bands as well as the M-shaped state emerge just below the bulk projected bands. Upon increasing the vdW expansion, these bands shift gradually down. This reflects the behaviour of the 2DEG bands as a function of the deposition time found in recent experimental studies [34, 38]. For expansions smaller than 10%, the PB is degenerate with the conduction bulk bottom band, however, for expansions of 10% and more, this state shifts into the energy gap. Up to 30%, the expansion also leads to a decrease of the effective mass m^* of PBs and to an increase of the Rashba coupling parameter α_R (see table 1). At the same time, m^* demonstrates an apparent $\bar{\Gamma}$–$\bar{K}$/$\bar{\Gamma}$–$\bar{M}$ anisotropy at 10% expansion. At higher expansions this anisotropy is significantly reduced. The small (≈ 0.01) m^* anisotropy, was also obtained in [40](SI). Different fitting procedures for the ARPES measured band in [40](SI), gave a Rashba splitting parameter varying from 0.36 to 1.35 eV Å for the aged Bi_2Se_3 surface. In the case of potassium deposition on Bi_2Se_3, a maximal $\alpha_R = 0.79 \pm 0.03$ eV Å was observed after 2.5–3 min of K evaporation [37]. Our model gives a lower limit for the former case at moderate expansions and underestimates the latter α_R, while the band-bending model [40] gives 0.1 eV Å for the PB splitting.

The nature of spin-split PBs can be deduced from an analysis of their spacial localization. At a 10% expansion, the emerged parabolic state still keeps a bulk-like delocalized character (figure 2(a)). This explains the obtained $\bar{\Gamma}$–$\bar{K}$/$\bar{\Gamma}$–$\bar{M}$ anisotropy of the PB at small expansions: it just reflects a similar anisotropy of the bulk states. Upon increasing the vdW spacings, this state

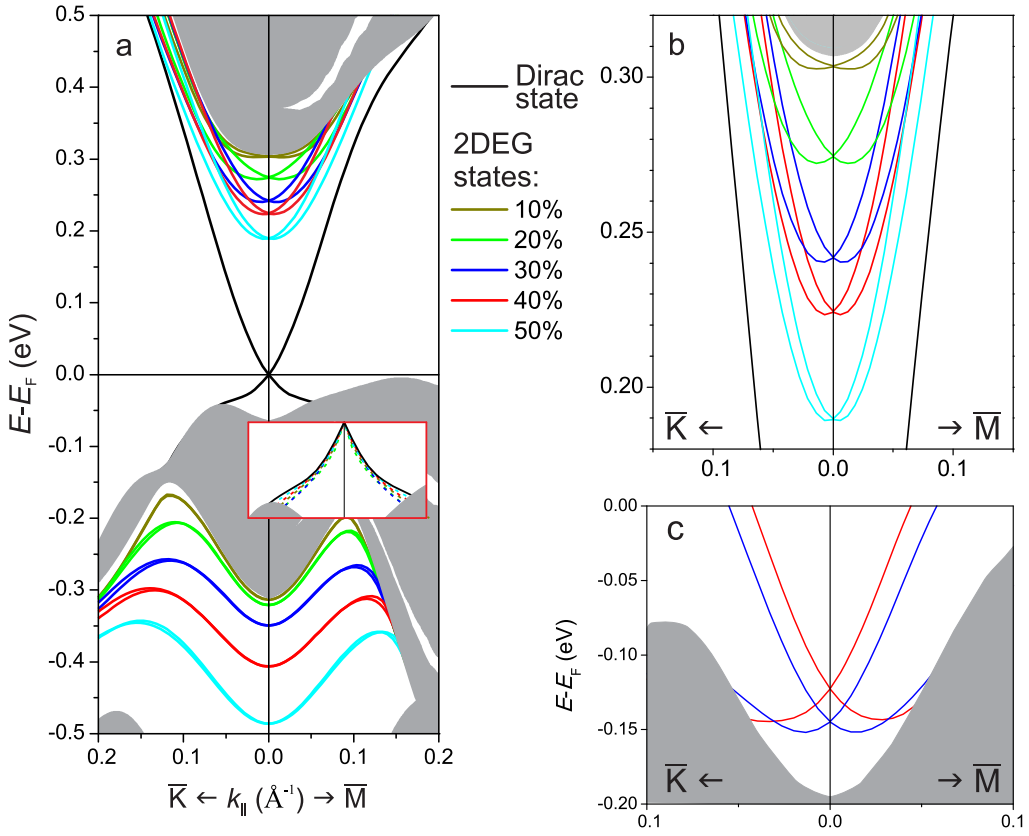

Figure 1. (a) The surface band structure of Bi_2Se_3 of a 9QL slab in the vicinity of $\bar{\Gamma}$ with the vdW gap expanded from 10 to 50% (inset: variation of the lower part of the Dirac cone with vdW gap expansion); (b) a magnified view of the Rashba-split PBs; (c) the Dirac cone on the ideal Bi_2Te_3 surface (blue) and with the 20% expanded vdW gap (red). The grey areas in (a)–(c) depict the projection of the bulk states onto the two-dimensional Brillouin zone.

acquires a more localized character and at 30–50% it almost completely lies in the detached QL. The PB state charge density distribution, characterized by four peaks localized in the outermost QL, figure 2(a), reflects the symmetry of the energy gap edges at $\bar{\Gamma}$: it is composed of the Bi p_z orbitals (the lower edge of the gap) with the sizeable Se p_z contribution (the upper edge of the gap) to the vdW-side peak (figure 2(b)). With a further increase in the outermost vdW spacing, the localization of the parabolic state approaches the distribution $|\Psi(z)|^2$ of the lowest unoccupied band in a free-standing QL (figure 2(c)). The latter band is not spin–orbit split, since a free-standing QL possesses inversion symmetry. This effect accounts for the reduction of α_R in the PB states with an increase in the vdW spacing beyond 30% (table 1). Note here that a large concentration of intercalated atoms in the vdW gap can affect the vdW-side Se orbitals and hence lead to a change in some features of the spin-split band, for instance the increase of Rashba splitting.

An intriguing finding is that the development of PB states is accompanied by the shifting of the topological state deep into the crystal, so that at a 30–50% expansion, the Dirac state is mostly located in the second QL, beneath the detached QL. In this case, wave functions of the topological and parabolic states only slightly overlap. The latter explains the

Table 1. The energy with respect to E_F, the fitted effective mass and the Rashba coupling parameter α_R for the parabolic SS as a function of the vdW gap expansion.

	Expansion	E_0	m^*		α_R (eV Å)	
	(%)	(eV)	$\bar{\Gamma}-\bar{K}$	$\bar{\Gamma}-\bar{M}$	$\bar{\Gamma}-\bar{K}$	$\bar{\Gamma}-\bar{M}$
Bi_2Se_3	10	0.30	0.38	0.46	0.16	0.14
	20	0.27	0.27	0.28	0.25	0.24
	30	0.24	0.20	0.20	0.33	0.32
	40	0.22	0.18	0.18	0.29	0.29
	50	0.19	0.17	0.17	0.24	0.24
Bi_2Te_3	20	0.075	0.32	0.30	0.51	0.50
	30	0.016	0.23	0.20	0.52	0.47
	40	−0.005	0.20	0.19	0.34	0.32
	50	−0.060	0.19	0.19	0.19	0.17
Sb_2Te_3	10	0.09	0.24	0.28	0.30	0.30
	20	0.08	0.17	0.18	0.35	0.36
	30	0.05	0.12	0.13	0.26	0.26
	40	0.04	0.12	0.12	0.15	0.15
	50	0.02	0.12	0.12	0.10	0.10
Bi_2Te_2Se	10	0.23	0.31	0.39	0.37	0.36
	20	0.15	0.18	0.2	0.44	0.46
	30	0.07	0.15	0.15	0.48	0.50
	40	0.02	0.13	0.12	0.48	0.49
	50	−0.01	0.10	0.10	0.40	0.38
Bi_2Te_2S	20	0.19	0.16	0.16	0.37	0.40
	30	0.14	0.13	0.12	0.37	0.37
	40	0.10	0.11	0.11	0.27	0.27
	50	0.08	0.10	0.10	0.16	0.17
Sb_2Te_2Se	20	0.25	0.58	0.59	0.09	0.09
	30	0.20	0.42	0.42	0.09	0.09
	40	0.18	0.37	0.37	0.06	0.07
	50	0.16	0.37	0.37	0.03	0.04
Sb_2Te_2S	20	0.23	0.61	0.61	0.02	0.02
	30	0.21	0.25	0.25	0.03	0.03
	40	0.20	0.23	0.23	0.02	0.02
	50	0.15	0.19	0.19	0.01	0.01
$PbBi_2Te_4$	10	0.11	0.66	0.57	0.14	0.20
	20	0.03	0.32	0.33	0.41	0.45
	30	0.01	0.32	0.32	0.32	0.31
	40	0.00	0.37	0.36	0.12	0.11
	50	−0.01	0.39	0.38	0.06	0.05

experimentally observed absence of inter-band scattering [34, 43]. It should be stressed that the dispersion of the upper part of the Dirac cone as well as the position of the Dirac point, with respect to the valence band edge, remain unchanged under this relocation. This behaviour is in

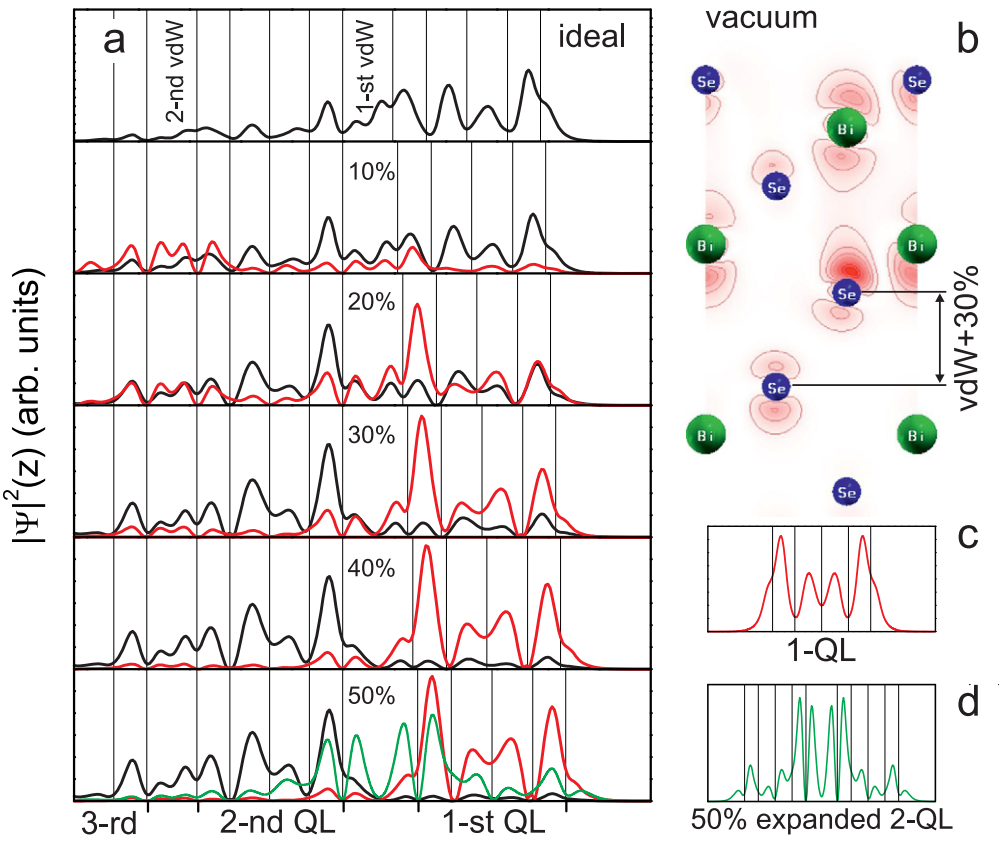

Figure 2. (a) Spatial localization of the topological (black) and parabolic (red) SS as a function of the vdW gap expansion; the green line represents localization of the M-shaped band for 50% vdW gap expansion; (b) the charge density distribution of the PB state for a 30% expansion; (c) and (d) $|\Psi(z)|^2$ of the lowest unoccupied band for a free-standing 1-QL and of the upper occupied band for a free-standing 2-QL with a 50% vdW gap expanded, respectively.

agreement with overall ARPES results and is in contrast with a band-bending simulation where the Dirac point becomes buried deep under the valence band edge [41]. At the same time the calculated dispersion of the lower part of the Dirac cone is slightly modified (figure 1(a), inset) in agreement with the ARPES data [36].

The M-shaped band emerges in the local gap of the bulk-projected valence band, splitting off from the upper edge of the gap. The edge formed solely by the bulk Se p_z states, which are not spin–orbit split at $\bar{\Gamma}$ and around. The M-shaped SS being split off from the Se p_z bands does not acquire any other symmetry and thus does not show spin–orbit splitting at small momenta. Only when it is close to the bulk continuum states (at large momenta), does it show weak spin–orbit splitting. With an increase in the vdW gap, it becomes more localized. Charge density of this state as shown for the 50% expansion case in figure 2(a) is mostly situated in the expanded vdW gap and around. Comparing this $|\Psi(z)|^2$ with that of the upper occupied state in the free-standing 2-QL with a 50% vdW gap expanded, figure 2(d), one notes that these two states are of the same origin: the vdW spacing expansion.

Now we consider the effect of the simultaneous expansion of the first and second vdW spacings. The expansion of the latter can be caused by further diffusion in the sample of a

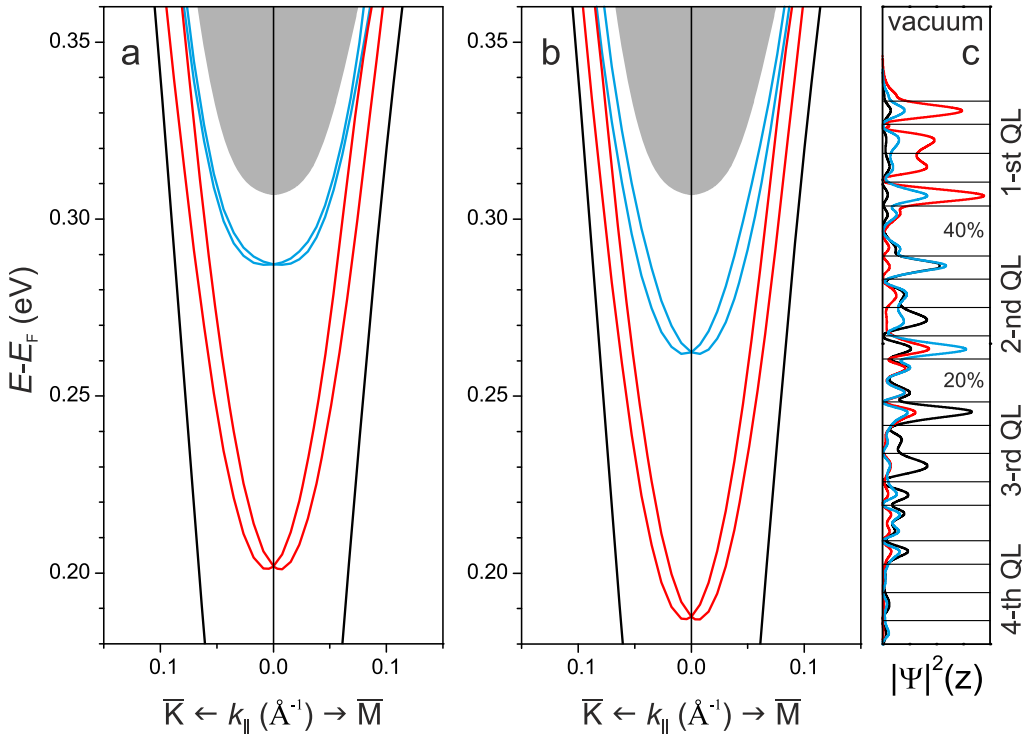

Figure 3. The surface band structure of Bi_2Se_3 with the first and second vdW gaps expanded by 40 and 10%, respectively (a); by 40 and 20%, respectively (b); and (c), spatial localization of the topological state (black line) as well as for the lower (red) and upper (blue) Rashba-split SS's for the (b) case.

smaller amount of atoms deposited on the surface. In figure 3(a) we show the band spectrum of Bi_2Se_3 with 40 and 10% expanded first and second vdW spacings, respectively. This film geometry gives rise to the second parabolic state below the conduction band. This state shows very small spin-splitting. The emergence of the second PB leads to a decrease in energy of the first band by 20 meV as well as a reduction of its α_R to 0.27 eV Å compared to the case of the single vdW spacing expansion by 40%. A further increase in the second vdW gap leads to a subsequent downshift of both PBs (figure 3(b)). While α_R for the upper band in this case is 0.16(0.15) eV Å in $\bar{\Gamma}$–$\bar{K}$ ($\bar{\Gamma}$–$\bar{M}$) directions, respectively, the spin-splitting of the lower state is reduced to 0.25 eV Å. Localizations of the lower and upper bands, in general, resemble those for a single vdW expansion by 40 and 20%, respectively, except in their mutual overlap (figure 3(c)). The overlap of the topological SS with that localized in the second QL, is similar to that in the single 20% case while the Dirac state is absent in the outermost QL as in the case of the single 40% detachment. A further increase in the second vdW spacing leads to a bigger downshift of both PBs, increasing their overlap and relocating the Dirac state to the third QL. The expansion of the second vdW gap also results in the development of a second M-shaped state in the valence band gap (not shown). Subsequently, expansion of the third vdW gap, that simulates a deeper diffusion of deposited atoms, leads to the simultaneous emergence of the third pair of parabolic Rashba-split and M-shaped bands (not shown).

Note that the sizeable overlap between the topological SS and 2DEG state exists barely at the beginning of the formation of each new PB and, hence the inter-band scattering is only

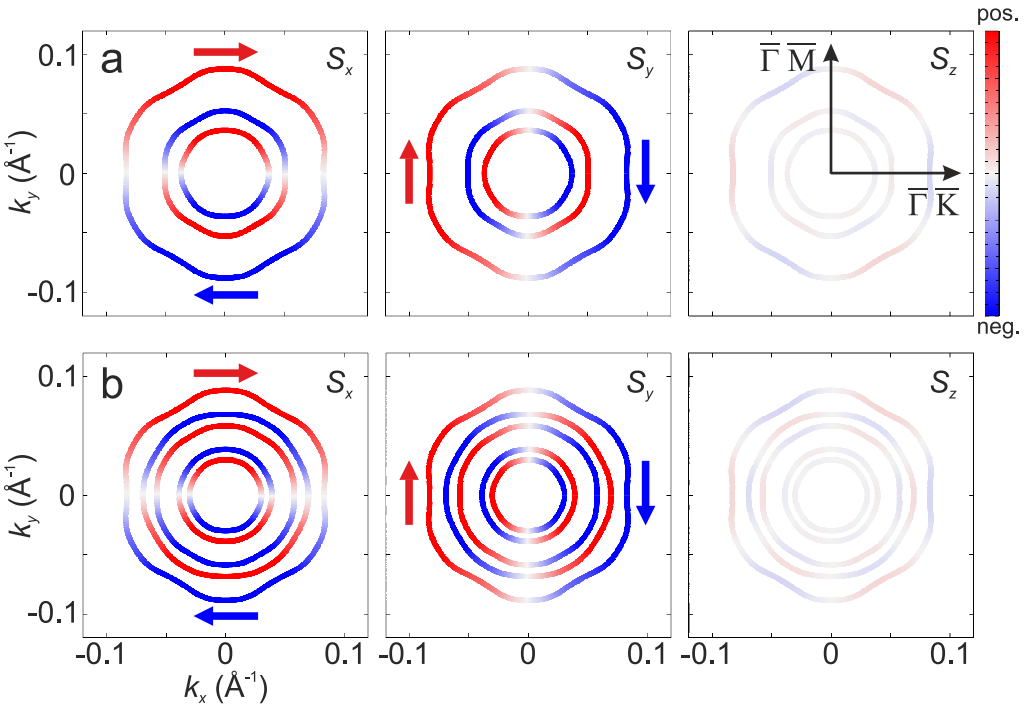

Figure 4. Spin structure of the Dirac state and Rashba-split states of Bi_2Se_3, as given by the spin projections S_x, S_y and S_z at an energy of 280 meV for the detached 1QL (30%) case (a) and for the 2QL (40 + 20%) case (b).

possible in a narrow energy interval just below the conduction band. In fact this scattering will be also limited by the spin conservation rule due to the spin-polarized nature of both the topological and the 2DEG Rashba-split states. The Dirac state has a clockwise spin helicity while the parabolic states demonstrate typical Rashba-type counter-clockwise and clockwise helicities for the outer and inner branches, respectively, with a small but discernible S_z spin component for both types of SS's (figure 4(a)). This spin structure allows '$\mathbf{k}_1$ to $\mathbf{k}_2$' scattering between the topological state and the inner branch of the PB and '$\mathbf{k}_1$ to $-\mathbf{k}_2$' transitions between the Dirac cone state and the outer branch of the PB. However, the efficiency of these transitions should be significantly reduced because of the small overlap between the topological SS and PB state for well-developed PBs. In the case of multiple detached vdW gaps, new channels for scattering of Dirac electrons (figure 4(b)) arise, nevertheless, only PBs that have a sizeable overlap with the topological SS can contribute to considerable inter-band scattering.

In order to confirm that the emergence of PBs upon the vdW expansion is an inherent feature of the layered TIs, we now perform calculations of the band structure of other binary TI (Bi_2Te_3, Sb_2Te_3) and ternary TI Bi_2Te_2Se, Bi_2Te_2S, Sb_2Te_2Se, Sb_2Te_2S as well as $PbBi_2Te_4$ having an SL layered structure under this effect. The former ternary compounds are characterized, like the Bi_2Se_3, by a tetradymite-like structure where the central layer in each quintuple block is replaced by Se or S, a slab of 9QL has been considered in all cases. The $PbBi_2Te_4$, which recently was verified as TI [31] by ARPES, also has a layered structure, but in this case the unit of repetition is a septuple layer (SL) block (Te–Bi–Te–Pb–Te–Bi–Te). For the latter system we have considered a slab of 49 atomic layers.

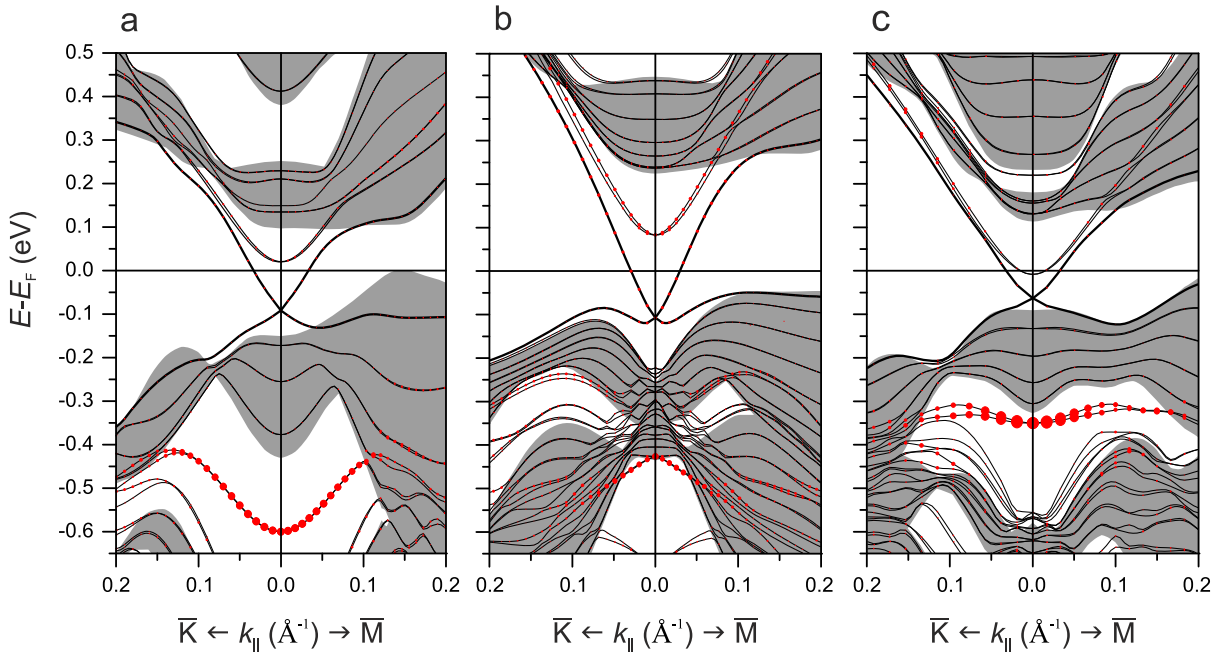

Figure 5. The surface band structure of Sb_2Te_3 (a), Bi_2Te_2S (b) and $PbBi_2Te_4$ (c) with the first vdW gap expanded by 50%. The size of the red circles denotes the weight of the p_z states localized at the bordering atoms of the expanded vdW gap. The projected bulk band structure is shown in grey.

First we consider the QL-structured compounds. For all these compounds we have expanded the outermost vdW gap from 10 to 50% and analysed the electronic structure. In all cases, vdW expansion causes the formation of new states in the conduction band, as in the former case Bi_2Se_3 (table 1). The difference is that in several compounds (Bi_2Te_2S, Sb_2Te_2Se, Sb_2Te_2S) at a 10% vdW expansion, the PB state does not appear below the projection of the bulk conduction band. We have studied the case of Bi_2Te_3 in detail earlier [58] and here we reproduce the obtained data in table 1. Mostly, we find the same trend in the development of the Rashba-split PB, but, as expected, a heavier Te provides a two times bigger α_R in Bi_2Te_3 compared to that of Bi_2Se_3. Nevertheless, Bi_2Te_3 presents, resulting from vdW expansions, some considerable differences concerning the Dirac cone with respect to Bi_2Se_3: we observe a displacement of the crossing point and that the dispersion of the lower/upper part of the cone differs with respect to the ideal case (figure 1(c)). The most prominent changes in the Dirac cone dispersion in Bi_2Te_3 occur at a 20–30% expansion, they become smaller for larger expansions when the topological state is completely relocated in the second QL. Sb_2Te_3 reproduces the same behaviour for PB and M-shaped bands as Bi_2Se_3 (see figure 5(a) where the weights of the M-shaped states at the bordering atoms of the expanded vdW gap are shown also).

The substitution of Te by S or Se in the central layer of the Bi_2Te_3 QL does not change the character of the gap, but it produces its broadening compared to the parent compound. The results we obtain for Bi_2Te_2Se and Bi_2Te_2S ternary compounds (table 1) are similar to Bi_2Te_3 with the only difference being that a smaller SOC due to the lighter third element results in a smaller Rashba parameter as compared to Bi_2Te_3. For these compounds we also observe the displacement of the Dirac point with respect to the ideal position. For Sb_2Te_2Se and Sb_2Te_2S a, the smaller SOC due to the lighter third element, also leads to a smaller Rashba parameter

(see table 1). In Sb-based systems the upper cone dispersion and the Dirac point remain identical to that in the ideal case. A difference between binary and ternary compounds (Bi_2Te_2S, Sb_2Te_2Se, Sb_2Te_2S) is the absence of the $\bar{\Gamma}$ bulk valence gap below the Dirac point. In these compounds, instead of the M-shaped band, we find a valence resonant state, which becomes a surface state in a deeper local gap at the large expansions (figure 5(b)).

In the case of $PbBi_2Te_4$ (figure 5(c)), the detachment of the outermost SL leads to two simultaneous effects: on one side we observe the emergence of the Rashba split bands below the bottom of the bulk conduction band (see table 1), and on the other side we can see a displacement of the Dirac point with respect to the ideal position as in Bi_2Te_3. As in the previous cases, the Dirac state is relocated to the second block.

To finalize, we performed calculations of other (non-topological) layered materials: we checked this effect for In_2Se_3 and Sb_2Se_2Te which have the same QL crystal structure as Bi_2Se_3 and are not TIs. In these compounds, even at large vdW expansion, the PB states do not appear. To clarify this point further, we also performed the calculation of Bi_2Se_3 without the inclusion of the spin–orbit coupling. In this case the vdW gap expansion gives rise only to the formation of the M-shaped bands while the PB states do not emerge in the band-gap. Thus, a strong SOC, which inverts band-gap edges in the TIs, is essential for the formation of the PB states. In_2Se_3 and Sb_2Se_2Te can be good test systems to prove this finding experimentally.

It should be noted that *n*-doping provided by adsorbates, which is a core of the band-bending approach, is not directly accounted for in our model. However, the band-bending effect does not contradict our results. As was shown in [40, 41], the band-bending effect also leads to the emergence of 2DEG states. The latter means that the band-bending effect would enhance the splitting of 2DEG states and as a result, the same energies of PB and M-shaped states, as well as the magnitude of the Rashba splitting in the latter bands should be realized at lower intercalation expansions. On the other hand the band-bending effect should primarily affect the near surface localized 2DEG states while the relocation of the Dirac state to the deeper QLs, as obtained in our model, preserves its gapless nature and almost unchanged dispersion. This differs from the results of the pure band-bending simulations [40, 41] which give the splitting the Dirac state of the bulk conduction band and results in the Dirac point being buried deep into the valence band.

A strong corroboration of our model comes from the temperature behaviour of the ARPES picture. In a recent work [39], it was shown that *n*-doping provided by exposure of the TIs to air or N_2 at 30 K, is partly reversed by annealing to 300 K. Under annealing, the Fermi level moves down (the Dirac cone shifts to smaller binding energies in the ARPES map) while 2DEG states remained almost unchanged with temperature. The shift of the Fermi level under annealing towards its location on the freshly cleaved surface is explained by the desorption process which results in electron removal from the surface. Whereas the insensitivity of the 2DEG states to the temperature increasing, is easily explained within our model: a portion of contaminants that has intercalated into the vdW gaps and which is responsible for the emergence of the 2DEG states cannot be recovered and desorbed at 300 K, in contrast to the rest of the contaminants remaining on the surface.

3. Summary and conclusions

To summarize, on the base of *ab initio* calculation results, we show that the intercalational expansion of vdW spacings in the layered TI's leads to the simultaneous emergence of parabolic

and M-shaped bands as well as Rashba-splitting of the former bands. These bands are 2DEG states localized in the narrow (sub)surface region. We find that in addition to the development of 2DEG SS's, the expansion of the vdW gap also provides the relocation of the topological state to the lower QL(SL). This fact explains the observed absence of inter-band scattering between the topological SS and Rashba-split PB states. We have also shown that expansion of the low-lying vdW gaps produces multiple 2DEG states. The proposed mechanism is valid for numerous layered TIs. Thus, the evolution of the surface electronic structure of the layered TI under an ambient environment or after the deposition of different adsorbates, cannot be explained by a simple band-bending model only. The evolution is more complex, requiring one to take into account a general effect for all layered materials such as the intercalation of the impurities into the vdW gaps.

Acknowledgments

We acknowledge partial support from the University of the Basque Country (project GV-UPV/EHU, grant no. IT-366-07) and the Ministerio de Ciencia e Inovación (grant no. FIS2010-19609-C02-00). Calculations were performed on the Arina supercomputer of the University of the Basque Country. We thank Ph Hofmann, A Kimura, Yu M Koroteev, E E Krasovskii and S S Tsirkin for enjoyable discussions.

References

[1] Fu L, Kane C L and Mele E J 2007 *Phys. Rev. Lett.* **98** 106803
[2] Fu L and Kane C L 2007 *Phys. Rev.* B **76** 045302
[3] Zhang H *et al* 2009 *Nature Phys.* **5** 438
[4] Chadov S *et al* 2010 *Nature Mater.* **9** 541
[5] Lin H *et al* 2010 *Nature Mater.* **9** 546
[6] Eremeev S V, Koroteev Yu M and Chulkov E V 2010 *JETP Lett.* **91** 594
[7] Lin H *et al* 2010 *Phys. Rev. Lett.* **105** 036404
[8] Kuroda K *et al* 2010 *Phys. Rev. Lett.* **105** 146801
[9] Eremeev S V, Koroteev Yu M and Chulkov E V 2010 *JETP Lett.* **92** 161
[10] Xia Y *et al* 2009 *Nature Phys.* **5** 398
[11] Chen Y L *et al* 2009 *Science* **325** 178
[12] Zhang T *et al* 2009 *Phys. Rev. Lett.* **103** 266803
[13] Kuroda K *et al* 2010 *Phys. Rev. Lett.* **105** 076802
[14] Eremeev S V, Koroteev Yu M and Chulkov E V 2010 *JETP Lett.* **91** 387
[15] Zhang Y *et al* 2010 *Nature Phys.* **6** 584
[16] Song J-H, Jin H and Freeman A J 2010 *Phys. Rev. Lett.* **105** 096403
[17] Zhang W *et al* 2010 *New J. Phys.* **12** 065013
[18] Yazyev O V, Moore J E and Louie S G 2010 *Phys. Rev. Lett.* **105** 266806
[19] Menshchikova T V *et al* 2011 *JETP Lett.* **93** 15
[20] Xu S-Y *et al* 2010 arXiv:1007.5111
[21] Silkin I V *et al* 2011 *JETP Lett.* **94** 217
[22] Arakane T *et al* 2012 *Nature Commun.* **3** 636
[23] Ren Z *et al* 2010 *Phys. Rev.* B **82** 241306
[24] Dai X-Q *et al* 2012 *J. Phys.: Condens. Matter* **24** 035502
[25] Wang L L and Johnson D D 2011 *Phys. Rev.* B **83** 241309

[26] Jia S *et al* 2011 *Phys. Rev.* B **84** 235206
[27] Lin H *et al* 2011 *New J. Phys.* **13** 095005
[28] Miyamoto K *et al* 2012 *Phys. Rev. Lett.* **109** 166802
[29] Neupane M *et al* 2012 *Phys. Rev.* B **85** 235406
[30] Eremeev S V *et al* 2012 *Nature Commun.* **3** 635
[31] Kuroda K *et al* 2012 *Phys. Rev. Lett.* **108** 206803
[32] Bianchi M *et al* 2010 *Nature Commun.* **1** 128
[33] Wray L A *et al* 2011 *Nature Phys.* **7** 32
[34] Valla T *et al* 2012 *Phys. Rev. Lett.* **108** 117601
[35] Scholz M R *et al* 2012 *Phys. Rev. Lett.* **108** 256810
[36] Wray L A *et al* 2011 arXiv:1105.4794v1
[37] Zhu Z-H *et al* 2011 *Phys. Rev. Lett.* **107** 186405
[38] Hadj Benia M *et al* 2011 *Phys. Rev. Lett.* **107** 177602
[39] Chen C *et al* 2012 *Proc. Natl Acad. Sci. USA* **109** 3694
[40] King P D C *et al* 2011 *Phys. Rev. Lett.* **107** 096802
[41] Bahramy M S *et al* 2012 arXiv:1206.0564v1
[42] Richter W, Kohler H and Becker C R 1977 *Phys. Status Solidi* b **84** 619
[43] Park S R *et al* 2010 *Phys. Rev.* B **81** 041405
[44] Dresselhaus M S and Dresselhaus G 2002 *Adv. Phys.* **51** 1
[45] Friend R H and Yoffe A D 1987 *Adv. Phys.* **36** 1
[46] Dresselhaus M S (ed) 1986 *Intercalation in Layered Materials* (New York: Plenum)
[47] Coehoorn R *et al* 1987 *Phys. Rev.* B **35** 6195
[48] Zak A *et al* 2001 *J. Am. Chem. Soc.* **124** 4747
[49] Kopnov F *et al* 2008 *Chem. Mater* **20** 4099
[50] Wang Y-L *et al* 2011 *Phys. Rev.* B **84** 075335
[51] Ye M *et al* 2011 arXiv:1112.5869
[52] Perdew P, Burke K and Ernzerhof M 1996 *Phys. Rev. Lett.* **77** 3865
[53] Kresse G and Furthmüller J 1996 *Phys. Rev.* B **54** 11169
[54] Kresse G and Joubert D 1999 *Phys. Rev.* B **59** 1758
[55] Blöchl E 1994 *Phys. Rev.* B **50** 17953
[56] Koelling D and Harmon B N 1977 *J. Phys. C: Solid State Phys.* **10** 3107
[57] Mishra S K, Satpathy S and Jepsen O 1997 *J. Phys.: Condens. Matter* **9** 461
[58] Vergniory M G *et al* 2012 *JETP Lett.* **95** 213